Journal of Sustainable Development of Energy, Water and Environment Systems

http://www.sdewes.org/jsdewes

Year 2026, Volume 14, Issue 3, 1140705

Original Research Article

A Novel Material for Nickel Removal: Magnetic Nanoparticles Supported on Dolomite

Tomás Lopez[1], Ana B. Fossati[2], Silvia E. Jacobo[2], Susana P. Boeykens[*1,3], María N. Piol[1,3]

[1] Universidad de Buenos Aires, Facultad de Ingeniería, Instituto de Química Aplicada a la Ingeniería (IQAI), Laboratorio de Química de Sistemas Heterogéneos (LaQuíSiHe), Buenos Aires, Argentina

[2] Universidad de Buenos Aires, Facultad de Ingeniería, Instituto de Química Aplicada a la Ingeniería (IQAI), Laboratorio Químico de Materiales Magnéticos Aplicados a la Ingeniería (LaQuíMMAI), Buenos Aires, Argentina

[3] Universidad de Buenos Aires, Facultad de Ingeniería, Instituto de Química Aplicada a la Ingeniería (IQAI), Grupo Interdisciplinario de Quimiodinámica (GIQuim), Buenos Aires, Argentina

e-mail: laquisihe@fi.uba.ar, gpo.LaQuiMMAI@fi.uba.ar, gpo.quimiodinamica@fi.uba.ar

Cite as: Lopez, T., Fossati, A.B., Jacobo, S. E., Boeykens, S.P., Piol, M.N., A novel material for Nickel removal: magnetic nanoparticles supported on dolomite, J.sustain. dev. energy water environ. syst., 14(3), 1140705, 2026, DOI: https://doi.org/10.13044/j.sdewes.d14.0705

ABSTRACT

This work aims to contribute to the development of new materials for environmental protection. The preparation and characterisation of new materials based on magnetic nanoparticles on a dolomite matrix are presented, along with an evaluation of their ability to remove nickel (II) from aqueous solutions. Different systems were prepared: pure dolomite, a mechanical mixture of dolomite with magnetic nanoparticles, and nanoparticles supported on a dolomite matrix. These systems were characterised, revealing distinct structural properties of the nanoparticles supported on a dolomite matrix. Tests were performed in batch and in continuous reactors under different operating conditions. These studies demonstrated a higher adsorption capacity for nanoparticles supported on a dolomite matrix. Removals of 39.6%, 17.4%, and 4.59% were obtained with nanoparticles supported on a dolomite matrix, magnetic nanoparticles mixed with dolomite, and dolomite alone, respectively. Furthermore, in fixed-bed reactors, nanoparticles supported on a dolomite matrix exhibited greater operational stability. These results position the nanoparticles supported on a dolomite matrix as a viable and safe option for treating industrial effluents.

KEYWORDS

Water treatment, Dolomite, Magnetic nanoparticle, Supported material, Nickel.

INTRODUCTION

The growth of industrial activity leads to an increase in the number of effluents that must be treated, with highly varied amounts and types of pollutants that depend mainly on the industry generating them. Among this list of pollutants, metals play a predominant role because they are non-biodegradable and, therefore, persistent in the environment [1]. Furthermore, they are bioaccumulative and can even biomagnify in the food chain, affecting populations not directly

* Corresponding author

exposed to the contamination source [2]. Some metals, such as nickel, are considered non-essential and may be carcinogenic [3]. Nickel can be found in effluents from various industries, such as steel, mining, and electroplating. Removing metals from effluents is a complex task that can be very costly economically. The success of the treatment depends not only on the removal of pollutants, but also on the viability of their use. In this sense, for its widespread use, it must be simple, effective, and low-cost. The pursuit of environmental compliance involves exploring these technologies to achieve ownership and, consequently, sustainability for those who use them. In this way, a lower economic cost would favour the direct reduction of environmental costs, at least with regard to effluent discharge. "Costs", according to Horngren *et al.* [4], are resources that are sacrificed or given up to achieve a specific objective; therefore, the challenge is not only to reduce economic costs but also to reduce the environmental costs associated with a process.

Various physical-chemical methods, such as chemical precipitation, solvent extraction, ion exchange and membrane separation, are effective for removing metals from water and effluents [5]. However, they have some disadvantages, such as incomplete treatment, high equipment and maintenance/monitoring costs, the need for chemical reagents and the generation of solid waste and sludge that require final disposal [6]. Another important disadvantage is their limited ability to treat high flow rates [7].

In addition to conventional effluent treatment, adsorptive processes offers advantages such as relatively low cost, simple design and easy operation [8]. These processes are surface phenomena that occur at the system interface through physical or chemical interactions. Adsorption is presented as a simple, economical, and flexible option for tertiary water treatment, both in design and operation. Adsorbents such as activated carbon, nanotubes, porous synthetic materials, and functionalised polymers are used for metal removal. All of these are often difficult to separate and regenerate, so the search for more efficient adsorbents with potential for reuse continues. Different types of adsorbents used for nickel removal include magnetic resins [9], chitosan nanocomposites [10] and magnetic zeolites [11] with yields of up to 99%. The selection of the adsorbent material requires special attention in the development and study of the process and will depend on its textural, morphological and physical-chemical characteristics, as well as its availability, cost, regeneration capacity and final disposal options [12].

New materials based on nanoparticles embedded in a porous matrix have been proposed for removing heavy metals from aqueous solutions. Ajala *et al*. [13] prepared titanium dioxide nanoparticles supported on acid-activated kaolinite clay to remove manganese (II), iron (III), lead (II) and copper (II) from mining wastewater. The anchoring of nanoparticles onto kaolinite clay enhanced the removal of the unwanted heavy metals. Liu *et al*. [14] prepared a novel potassium hydroxide-activated porous biochar embedded MgO composite to remove lead (II) and cadmium (II) from wastewater. This material exhibited a superior adsorption capacity compared to other materials reported in the literature. Feng *et al*. [15] fabricated a biomass carbon-activated composite by controlling the growth of nanoparticles on the surface of soybean pods, serving as a precursor to the carbon matrix, to remove caesium (I) from radioactive wastewater. The adsorption capacity of the composite was significantly increased due to the anchoring technology. Li *et al*. [16] synthesised porous cellulose/chitosan composite spheres loaded with nanoscale zero-valent iron for the removal of cadmium (II) from aqueous solution and contaminated soils. The material had great potential as an excellent adsorbent in cadmium (II) removal. Zhu *et al*. [17] developed a novel aminated lignin/geopolymer composite supported with iron nanoparticles for the adsorption of chromium (VI) and naphthalene from wastewater, demonstrating high removal potential. Since their ability to remove metal ions, nanofiltration membranes have emerged as attractive tools in water treatment technologies. For example, cellulose acetate membranes with amino acids and ionic liquids [18] and gradient cross-linking membranes [19] were tested for metals recovery.

In this scenario, magnetic nanoparticles are a promising alternative. They are easily synthesised and have a high capacity to remove large volumes of water in a short time [20]. They have been tested for various contaminants [21], and this efficiency is mainly due to their large surface area and structural characteristics. The problem of working with nanoparticles can arise when scaling up. Considering an industrial-scale project is the ultimate engineering goal, and it is where the disadvantages arise. Therefore, it is necessary to propose and test other alternative uses of these nanoparticles at the laboratory scale that may be useful for future extrapolations.

Considering a system as low cost can be seen with two meanings, on the one hand, the use of an economical adsorbent material in large quantities, among which dolomite can be used, which is a calcareous rock ($CaMg(CO_3)_2$) of great abundance in our country and which has been tested as a metal adsorbent. With a mix of dolomite and quartz-based magnetite (Fe_3O_4) a maximum removal of 95% for lead and 87% for cadmium was obtained [22]. Binary solutions were tested using a fixed-bed reactor filled with dolomite [23] and with dolomite mixed with banana peel as adsorbents [24], obtaining, in both cases, removals of 70% of chromium. Dolomite [25] and dolomite mixed with banana peel [24] were used for the phosphate removal, achieving 99% removal in both cases. On the other hand, a specific material can be used with high efficiency and relatively high cost, but in small quantities, such as magnetic nanoparticles, which have also been tested for oil recovery [7] or as pollutant removal agents for dyes [12], metals [20], copper [21], cadmium and lead removal [22]. The use of magnetic nanoparticles in large reactors is difficult to implement due to their small size. Therefore, this work proposes to leverage the benefits of magnetic nanotechnology to address the important challenge of scaling it up and applying it to the treatment of industrial effluents. To this end, a continuous fixed-bed system is proposed, composed of an accessible material, such as dolomite (a calcareous rock), with magnetite nanoparticles synthesised on it serving as reactor packing for nickel removal. While other authors [22] have proposed mixing materials, this work explores the advantage of attaching the nanoparticles to the inorganic material, ensuring their immobility. This concept translates into greater efficiency in contaminant removal and increased environmental safety, as the nanoparticles can be disposed of along with the bed in which they are embedded.

MATERIAL AND METHODS

Dolomite is a mineral composed of calcium and magnesium carbonate, whose chemical formula is expressed as $CaMg(CO_3)_2$. Dolomite used in this research was obtained as broken stone from quarries in the Olavarría District, Buenos Aires, Argentina. It was donated by the company QUIMIN S.A.$^{(R)}$. The material was washed with deionised water and dried, ground in a mortar and then sieved to obtain the required fraction using a tower of standard series sieves with mesh sizes No. 200, 270, 325, and 400 (74, 53, 44, and 37 μm) placed in order of decreasing opening size. For the tests, a particle size corresponding to the fraction 53–74 μm was used [26].

Synthesis of Magnetic Nanoparticles

For the synthesis of magnetite (Fe_3O_4) nanoparticles, a variation of the co-precipitation method reported by Fossati *et al.* [7] was used. Two solutions, denoted A and B, were prepared. Solution A was prepared by dissolving ferrous sulphate heptahydrate ($FeSO_4 \cdot 7H_2O$) in 40 mL of distilled water in a three-neck round-bottom flask under an inert atmosphere of nitrogen. Solution B was prepared by dissolving ferric chloride hexahydrate ($FeCl_3 \cdot 6H_2O$) in 40 mL of distilled water under a nitrogen atmosphere, then adding it to solution A. Both solutions were heated to 80°C under a nitrogen atmosphere with magnetic stirring for 30 min. Then, a solution of sodium hydroxide was slowly added to the solution, resulting in a pH of 11. After 45 min, the three-neck round-bottom flask was cooled at room temperature. An hour later, the system was placed on a magnet for 2 min, so the supernatant was discarded. The black powder

(precipitate) was washed 4 times with distilled water and twice with ethanol. The suspension was centrifuged at 1200 rpm for 5 minutes, then the supernatant was discarded. Finally, the precipitate was left to dry in a vacuum oven for 24 h at 30°C.

Synthesis of Magnetite Supported on Dolomite

100.0 mL of solutions of $FeCl_3 \cdot 6H_2O$ (0.500 M) and $FeSO_4 \cdot 7H_2O$ (0.275 M) were prepared to obtain approximately 25 g of magnetite supported on dolomite. The prepared solutions were mixed in a container that previously contained 20.00 g of washed and dried dolomite. The system was kept stirring in a nitrogen atmosphere in a thermostatic bath at 80°C for 30 minutes. Through a slow drip (0.5 mL min^{-1}), 50.0 mL of 2.90 M NaOH solution was added to the system. Then, 26.0 mL of the sodium hydroxide was added to the container (2 mL min^{-1}), reaching pH = 11. Once the procedure was completed, a multi-step washing process was performed. First, the system was washed 6 times with 300.0 mL of distilled water each time, then 2 times with ethanol, and finally once with acetone. Finally, the magnetic dolomite obtained was allowed to dry in a vacuum oven at 70°C. The sample obtained was weighed and reserved for later use.

Characterisation of the Adsorbents

The crystallinity of the samples was analysed by X-ray powder diffraction (XRD) using a Rigaku diffractometer with CuKα radiation, scanned over 2θ from 10º to 80°.

The release of impurities from the adsorbents was measured by the total reflection X-ray spectrometry technique (TXRF), using a PICOFOX S2 spectrometer, BRUKER (Germany) [26].

Powder samples pellets were mixed with potassium bromide (KBr) Thermo Spectra-Tech, Grade FT-IR 99+%) for Fourier Transform Infrared Spectroscopy (FTIR) analysis. Samples were pressed into a 3 mm disc using a Hand Press accessory from PIKE Technologies. Spectral data were collected with a resolution of 4 cm^{-1} over the range of 400–4000 cm^{-1} and 32 scans per sample [27].

The zero charge point (ZCP) method was used to determine the charge of active centres on the surface of a material in a determined solution [20]. It is defined as the pH at which the surface charge is zero. Results were plotted as ΔpH vs. pHi, and the pHi corresponding to the zero ordinate is the ZCP [28].

Scanning electronic microscopy (SEM) determinations for dolomite were made with an electronic scanning spectroscope (Zeiss, EVO MA). The equipment used to analyse the rest of the samples was a Zeiss GeminiSEM 360. Brunauer-Emmett-Teller (BET) surface area analysis was performed from nitrogen adsorption isotherms using a Micrometrics model ASAP 2020 adsorption analyser.

Adsorbate Quantification

The solutions used in the calibration curve were prepared by diluting standard solutions of 1000 mg $Ni \cdot L^{-1}$ (SCP SCIENCE™). To determine metal concentrations in solution, a GBC-XplorAA air-acetylene Flame Atomic Absorption spectrometer with a nickel hollow-cathode lamp (λ=232.0 nm) was used, following the standard method [29].

Discontinuous Reactor Tests

Three different types of adsorbents were tested: Dolomite (D), Magnetite nanoparticles supported on dolomite (SS) and a mechanical mixture of magnetite nanoparticles and dolomite (MM). Table 1 shows the composition of the samples and the nomenclature used.

The discontinuous tests were carried out using 1.50 g of combined adsorbent (1.35 g of D + 0.15 g of SS or MM) in agitation under controlled conditions with 50.0 mL of Ni^{2+} solution, prepared from $NiCl_2 \cdot 6H_2O$. The description and adjustment of the procedure were previously

reported [18]. To calculate the percentage removal, the initial concentration was subtracted from the equilibrium concentration, and the resulting value was expressed as a percentage of the initial concentration.

Table 1. Samples nomination and description

Nomination	Description
MN	Magnetite nanoparticles
D	Dolomite
SS (20%MN, 80%D)	Magnetite nanoparticles supported on dolomite
MM (20%MN+80%D)	Mechanical mixture of MN and D

The adsorbent's retention capacity (q) was calculated using eq. (1):

$$q = \frac{C_0 - C_{eq}}{m} \times V \quad (1)$$

where C_0 and C_{eq} are initial and equilibrium concentrations of Ni^{2+} (mM), respectively, V is the volume of solution, and m is the dry mass of the adsorbent.

To investigate the mechanism of adsorption processes, experimental data were fitted according to both the Langmuir [30] and the Freundlich [31] models. To fit the experimental data from the kinetic assays, pseudo-first-order and pseudo-second-order models were employed. The mathematical expression for the pseudo-first-order kinetic model [32] is widely used in adsorption studies of liquids. The pseudo-second order model was developed by Ho and McKay [33]. It is assumed that sorbate is adsorbed on two active sites on the sorbent. For data analysis, the OriginPro 2024® software package was used.

Continuous Tests

A tubular reactor made of acrylic material, with a volume of 26.5 cm^3, 15 cm in length and 1.5 cm in diameter, was used for the continuous tests (**Figure 1a**). These dimensions ensure that no obstructions, channelling or fluid overflows occur [34]. The concentration of the working solution was 30 mg Ni^{2+} L^{-1}.

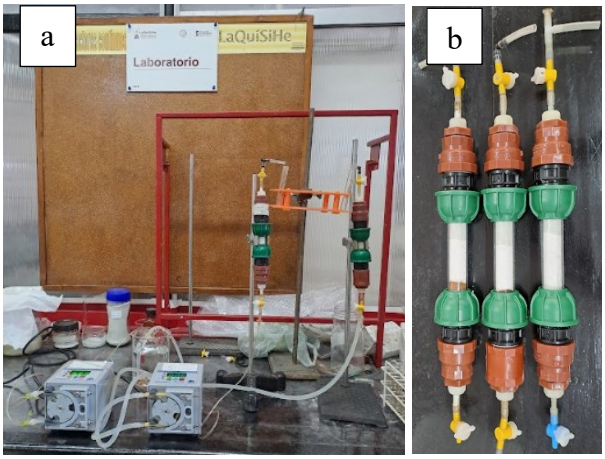

Figure 1. Continuous systems: complete system with two continuous ascending flow reactors (a), three reactors used for the comparison of different materials (D, SS and MM) as fillers (b)

The following mixture proportions of adsorbents were used as fillers: a) 1.25 g SS, and 12.5 g D; b) 1.25 g MM and 12.5 g D; and c) 13.7 g D (**Figure 1b**). These quantities ensure the same percentage of inorganic material and nanoparticles in reactors a and b.

Reactor c was used to determine the amount of nickel removed by D. A slow, low-flow rate (0.5 mL min^{-1}) of nickel solution was circulated to ensure contact between the contaminants and the adsorbent material. Samples were collected at the column outlet every 5 minutes. The reactor operates in piston flow, as previously demonstrated in a fluid-dynamic test with an inert material [35], to evaluate the dispersion module of the system, according to the Levenspiel criterion [36]. Once the breakthrough curves were obtained, the fits from Thomas [37], Adams-Bohart [38], and Yoon-Nelson [39] models were tested.

For data analysis, the OriginPro 2024® software package was used.

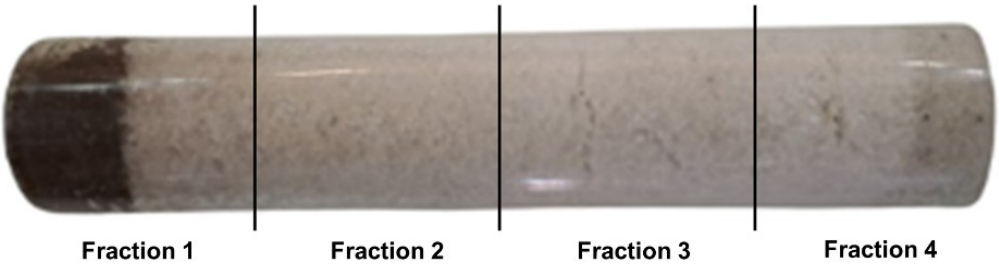

Figure 2. Fractions of the filler of the reactor a (SS+D)

For the analysis of the filler from the tubular reactor a (SS+D), the material was fractionated into four parts (Figure 2), each of which was digested to measure Ni^{2+} and iron concentrations.

The samples were dissolved in 50 mL of aqua regia (nitric acid, HNO_3, and hydrochloric acid, HCl) and heated (100°C) until the vapours ceased. Then, the samples were completely dissolved, reducing the volume to less than 10 mL. After transferring the solution to a 25 mL volumetric flask, the volume was made up to the mark with deionised water. Finally, the Ni^{2+} and iron concentrations in each sample were quantified.

RESULTS AND DISCUSSION

The crystalline structures of the prepared materials were investigated by XRD, and their comparative patterns are shown in Figure 3. The magnetite sample presents Bragg peaks that can be indexed to the cubic spinel structure (JCPDS 19-629) [40]. The dolomite sample shows characteristic Bragg peaks located at 2θ = 30° and 2θ = 40°. However, some unassigned absorption peaks are shown, which could be related to other impurities present in the natural rock.

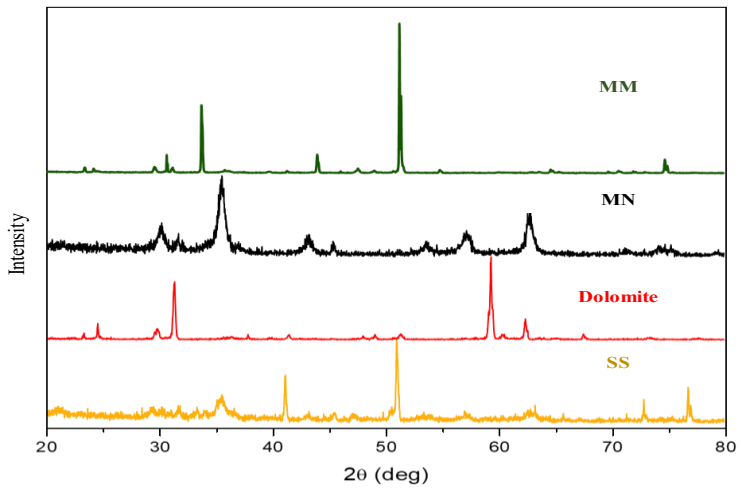

Figure 3. Diffraction patterns of magnetite nanoparticles (MN), dolomite (D), magnetite supported on dolomite (SS) and a mechanical mixture of MN and D (MM)

When comparing the magnetite supported on dolomite sample with the typical absorption peaks of dolomite, it is shown that dolomite is no longer present since the peak at 30°, the most intense reflection of the dolomite, almost completely disappears. This indicates that the synthesis performed on D allows a better distribution of the MN. Furthermore, peaks coinciding with magnetite are evident.

At 2θ = 50°, a new signal is observed in both MM and SS. In these two systems, characteristic signals of dolomite and NM, such as those appearing at 30° or 35°, disappear, and other signals appear that are repeated in both MM and SS. The differences in diffraction patterns indicate a strong interaction between dolomite and NM in both the MM and SS mixtures. Furthermore, the generation of new peaks could suggest the formation of a new material in the case of SS. Further studies could be initiated on this topic.

TXRF analysis was performed on a water sample that had been in contact with pure dolomite for 24 hours. Qualitative and quantitative analyses of the data, using cobalt as a calibration reference (international standard method), indicated that the main impurities released by the dolomite sample were strontium, calcium and magnesium. These studies suggest that dolomite does not release nickel or iron. Therefore, it could be used as a support material for nanoparticles and as a complementary filling material in continuous reactors for future tests, without posing a contamination risk.

Figure 4 shows FTIR spectra of the dolomite and magnetite nanoparticles. The main bands for the D are observed around 1400 and 800 cm^{-1}, indicating the presence of the CO_3^{2-} group.

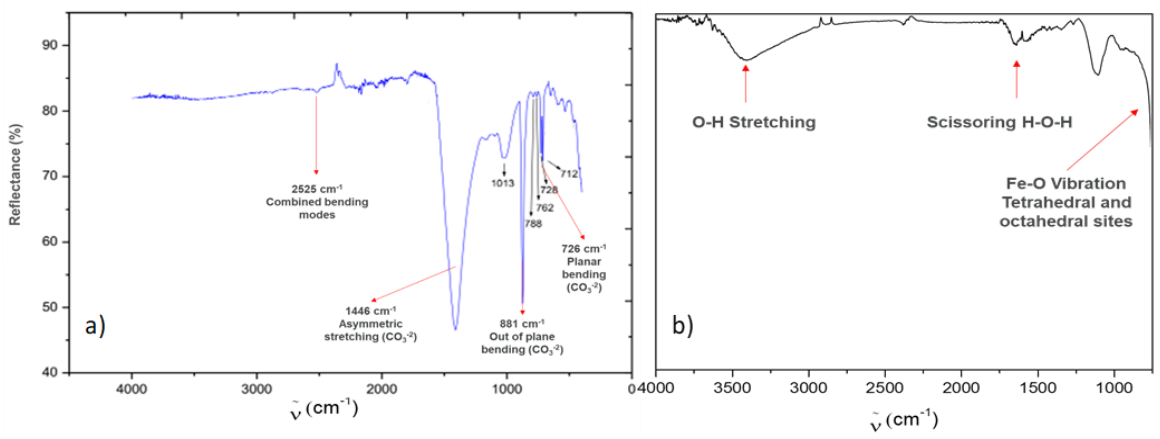

Figure 4. FTIR profiles for dolomite D (a) and magnetite nanoparticles MN (b)

Absorption at 726 cm^{-1} corresponds to in-plane bending; absorption at 881 cm^{-1} corresponds to out-of-plane bending. The absorption at 1446 cm^{-1} corresponds to asymmetric stretching, and at 2525 cm^{-1} corresponds to a combination of frequencies. An intense absorption is observed at 1013 cm^{-1} which could be due to silica or silicates [41]. The MN spectrum shows a broad band between 3100 and 3660 cm^{-1}, with a maximum at 3440 cm^{-1}, attributed to the O-H bonds stretching, indicating the presence of hydroxyl groups. Furthermore, a peak is observed at 1617 cm^{-1}, corresponding to the scissoring mode of vibration of the H-O-H bonds. These two bands are consistent with the presence of water molecules adsorbed on the nanoparticles' surfaces. The absorption band at 573 cm^{-1} is assigned to the Fe-O bond vibrations in tetrahedral and octahedral environments of their crystal structure. Weaker signals are observed at 890 and 800 cm^{-1}, which can be attributed to the presence of Fe-OH groups on the surface [20].

The results of zero charge pH tests are shown in **Figure 5a** and **Figure 5b**. For MN, the zero-charge pH is slightly acidic (6.54), while for the supported system, it is alkaline (8.35). For D, according to previous work from our laboratory, the zero-charge point was pH = 4.27 [24]. Since nickel has a positive charge and the working pH is 6.5, those adsorbents with a pH of zero charge below this value, as is the case with D and MN, are in a favourable situation,

whereas the opposite happens for the SS. The SS system has an even more promising perspective as a sorbent in basic media (above its zero-charge pH). According to the literature, the most favourable pH value to remove Pb^{2+} and Cd^{2+} is 8.5 [22]. This value is similar to the one obtained for the supported system.

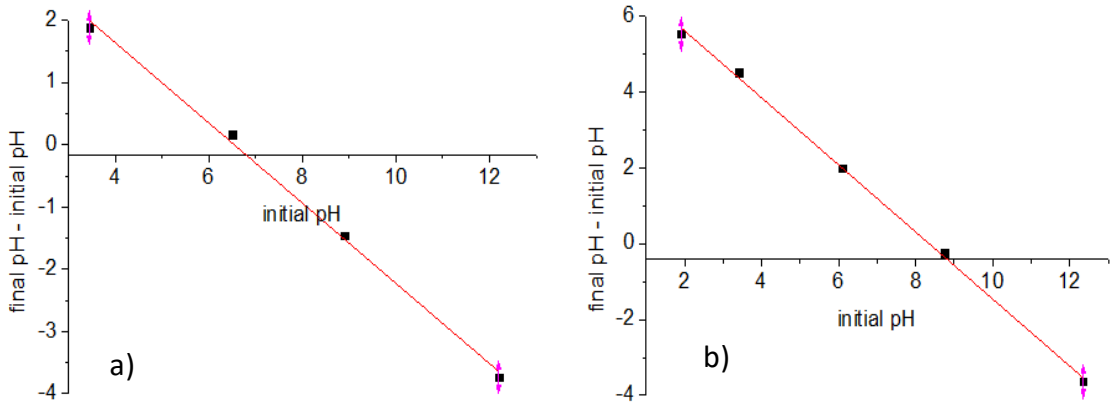

Figure 5. Zero charge pH test for magnetite nanoparticles MN (a); magnetite supported on dolomite SS (b)

Table 2 shows the BET surface area and the total pore volume for magnetite, dolomite, magnetite supported on dolomite and the mechanical mixture of dolomite and magnetite. It is shown that MN presents the largest specific surface area (80.7 m^2g^{-1}), quadrupling that of the SS system (19.03 m^2g^{-1}) and about two orders of magnitude larger than the MM (0.91 m^2g^{-1}). This situation could have occurred because, during mixing the D with the MN to obtain the MM system, the nanoparticles could have plugged the dolomite's pores. As a consequence, the surface area of the D decreases.

Table 2. BET surface area and total pore volume for the analysed samples

Sample	BET specific surface area [m^2g^{-1}]	Total pore volume [cm^3g^{-1}]
MN	80.70	0.2007
D	1.83	0.0030
SS	19.04	0.0095
MM	0.91	0.0005

When the MN are mechanically mixed, they agglomerate, significantly reducing their surface area. On the other hand, when performing the SS system, this would not occur. Therefore, it can be assumed that the great difference in surface areas between SS and MM would be due to an occupation of active sites of the MN by the D, generating a significant decrease in the exposed surface, a phenomenon that would not be happening when carrying out the synthesis of magnetite directly on the surface of the D. This assumption is also supported by the fact that D has a higher surface area than the MM system, so these two materials do not complement each other, but rather harm each other in terms of sorption capacity. Other authors also reported successful modification of dolomite with quartz for metal adsorption [22].

Figure 6 shows SEM images of the system obtained by mechanical mixing of dolomite and nanoparticles. Dolomite particles were highlighted in blue to facilitate their identification, and the smaller particles correspond to the nanoparticles. Particles present an average size of 15.5 nm, indicating that these particles are single-crystalline. In contrast, dolomite shows average particle sizes greater than 100 nm, which agrees with the narrow peaks observed in the diffractogram and confirms the absence of broadening due to crystalline-domain size.

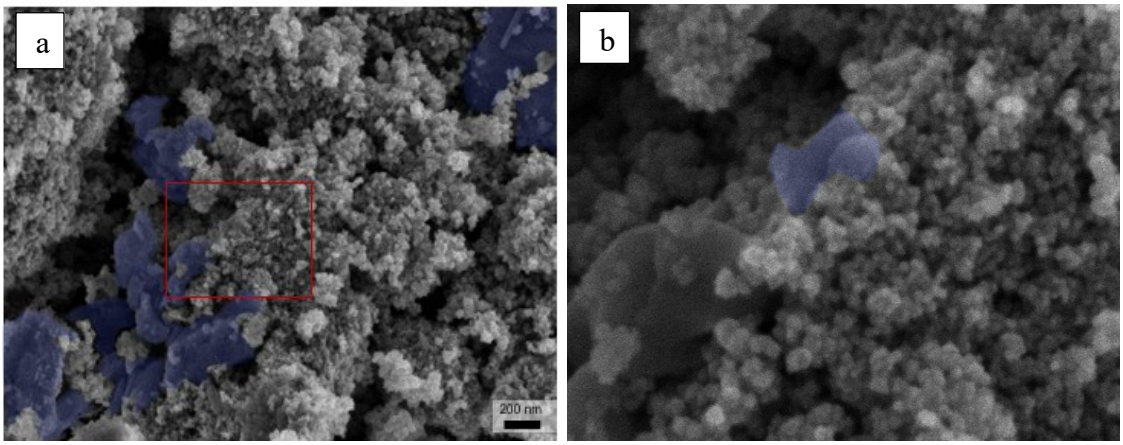

Figure 6. SEM images: magnetic nanoparticles + dolomite MM (a), and zoom of MM image (b)

Figure 7 presents a change in the MN distribution on the D surface. It suggests a variation in the material's chemical composition, which may result from the combination of D with MN through the surface hydroxyl group and the intermediate oxygen (-O-) in the carboxyl functional group **[22]**. The image shows nanoparticles attributed to magnetite (in red) and microcrystals with well-defined facets, corresponding to the dolomite substrate (in blue) after the partial dissolution of some of its constituent phases. Therefore, with a simple synthesis process, it was possible to obtain a new surface distribution of MN on D with a different surface area.

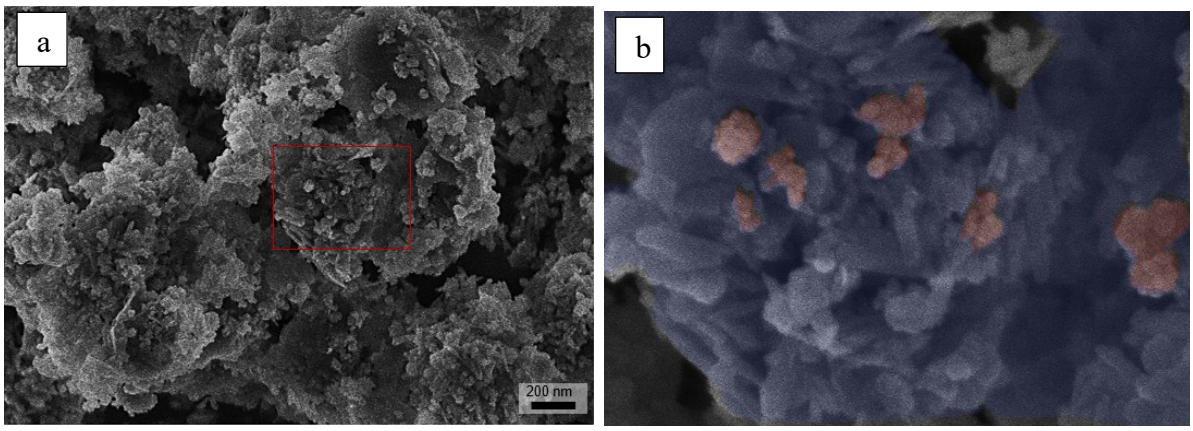

Figure 7. SEM images: magnetite supported on dolomite SS (a), and zoom of SS image (b)

Discontinuous Test

A comparison of removal efficiency is presented in **Figure 8**. While the other systems decrease their removal efficiency with increasing concentration, the D+SS system maintains constant total removal. At the same time, it has a higher percentage value (99%) than the rest for all the conditions studied. The Ni^{2+} concentration was increased to 130 mg L^{-1} and 400 mg L^{-1} to determine at which concentration the SS does not completely remove the ions present, thereby ensuring the working conditions.

The parameter q is the adsorption capacity or adsorbed load. It represents the amount of adsorbate that an adsorbent material can retain on its surface or in its pores. It is useful to compare the performance of the materials; therefore, the values of q, calculated for the materials used at each working Ni^{2+} concentration, are shown in **Figure 9**, where D+MM and D+SS indicate the combinations of dolomite-containing systems.

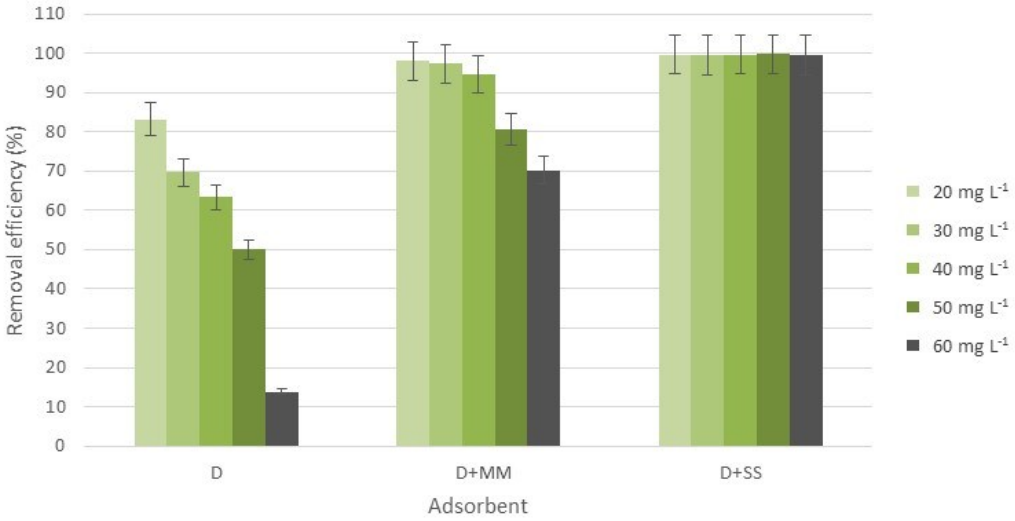

Figure 8. Comparison of removal efficiency by adsorbent for 20, 30, 40, 50 and 60 mg L-1

It is observed that as the adsorbate concentration increases (from 10 mg L^{-1} to 400 mg L^{-1}), the amount of metal adsorbed per mass of adsorbent is greater in all series. This is expected, since a higher adsorbate concentration increases the possibilities of adsorption. At low concentrations, large differences are observed between the series. The supported system (SS) has a significantly higher adsorption than the others, reaching approximately 0.13 mmol g^{-1}. For higher concentrations, MM and SS achieve the highest adsorption amounts. In particular, at 400 mg L^{-1}, MM and SS achieved their highest adsorption values of around 0.25 mmol g^{-1} and 0.32 mmol g^{-1}, respectively. These values were higher than those reported in the literature for nanoparticles synthesised on lignocellulosic materials [42] and those found for Cd^{2+} and Pb^{2+} on that adsorbent [22].

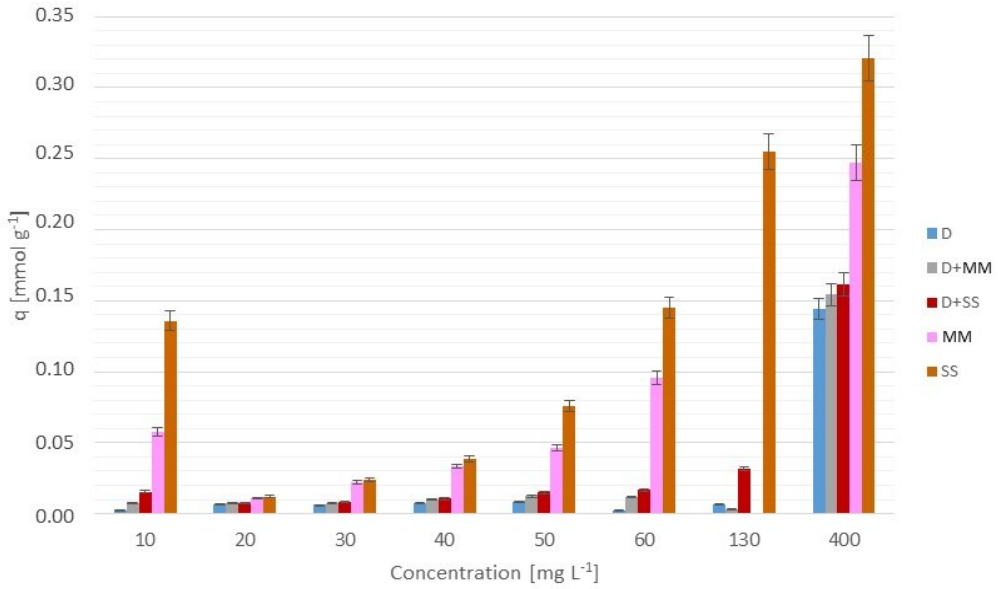

Figure 9. Adsorption capacity of Ni2+for the different adsorbent samples

Table 3 presents the parameters obtained from the Langmuir and the Freundlich isotherm models. The regression coefficients indicate that the best fit is Langmuir in all cases. It can be inferred that here, nickel ions are homogeneously arranged on the adsorbent surface (featuring identical active sites with the same adsorption energy) and form a single-layer coverage.

Table 4 shows the parameters obtained from the pseudo-first- and pseudo-second-order models fits of the experimental kinetics curves. The pseudo-second-order model assumes that the rate depends on the square of the number of unoccupied sites, and is best for describing chemisorption mechanisms. Here, the pseudo-second-order model is the best fit to the experimental data. Worth noting is that results similar to those shown in **Table 3** and **Table 4** have been reported in the literature for the removal of other metals using dolomite **[23]** and the mixture with nanoparticles **[22]**.

Table 3. Langmuir and Freundlich obtained parameters

Model	Langmuir			Freundlich		
System	Q_{max} [mmol g^{-1}]	K_L [L $mmol^{-1}$]	R^2	K_F	N	R^2
D	0.0102	11.0	0.978	0.0104	0.2564	0.906
MM+D	0.0123	157.0	0.971	0.0148	0.1361	0.894
SS+D	0.0330	199.0	0.904	0.4416	0.6215	0.899

Table 4. Pseudo-first- and pseudo-second-order models obtained parameters

Model	Pseudo-first-order			Pseudo-second-order		
System	q_e [mmol g^{-1}]	K_1 [min^{-1}]	R^2	q_e [mmol g^{-1}]	K_2 [mmol g^{-1} min^{-1}]	R^2
D	0.00340	0.179	0.788	0.00360	86.0	0.853
MM+D	0.00401	0.224	0.889	0.00479	75.9	0.949
SS+D	0.00600	1.10	0.999	0.00601	4600	0.999

Continuous Test

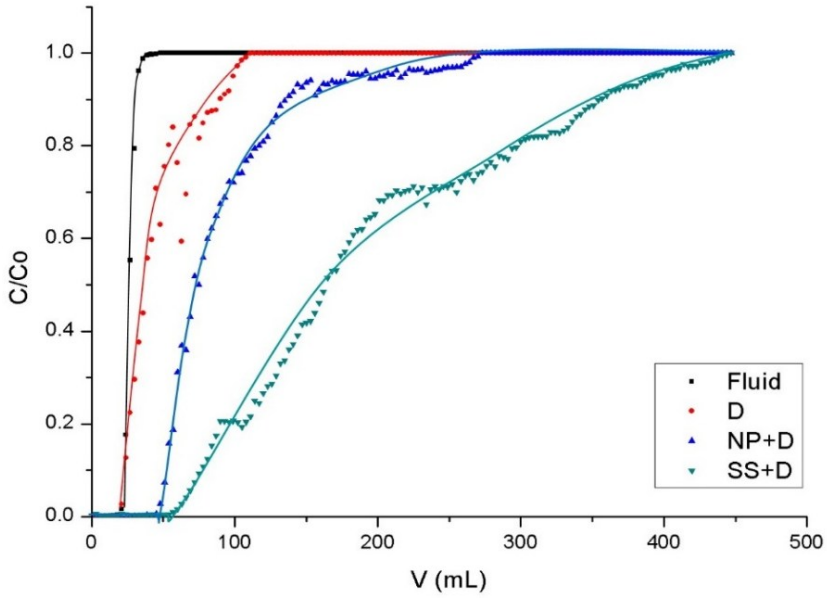

Figure 10. Experimental data obtained from the continuous reactor tests with different fillers

A fluid-dynamic test was performed to verify whether the behaviour of the continuous reactor could be approximated to an ideal plug flow. A value of 0.0088 was obtained for the dispersion modulus, so the ideal plug flow approximation is valid for the system under

study [43]. Figure 10 shows the breakthrough curves for all the systems studied, including the fluid-dynamic test curve.

Table 5 shows the results of the models used to fit the breakthrough curves. The models that best fit the results across all the systems are the Thomas and Adams-Bohart models, as confirmed by Vallini et al. [28] for nickel removal using demolition waste.

Table 5. Obtained parameters from the different models tested

Model	Thomas			Adams-Bohart			Yoon-Nelson		
System	K_{TH} [mL $min^{-1}g^{-1}$]	q_0 [mmol g^{-1}]	R^2	K_{AB} [cm^3 $mmol^{-1}$ min^{-1}]	N_0 [mmol cm^{-3}]	R^2	K_{YN} [min^{-1}]	T [min]	R^2
D	0.154 ±0.007	1.49 ±0.02	0.967	0.242 ±0.036	0.28 ±0.01	0.920	0.075 ±0.004	42.2 ±0.7	0.967
MM+D	0.108 ±0.004	2.85 ±0.03	0.982	0.16 ±0.02	0.55 ±0.01	0.914	0.052 ±0.002	80.3 ±0.8	0.982
SS+D	0.032 ±0.001	6.43 ±0.07	0.970	0.029 ±0.001	1.52 ±0.02	0.945	0.0158 ±0.0005	182 ±2	0.970

Subsequently, the area under the curves was estimated to determine the amount of nickel retained in the continuous reactor filler. The results of comparing the tests using D, MM, and SS show a good correlation with those obtained in the discontinuous system, with the SS having greater efficiency.

Table 6 shows, for each system, the total volume of solution fed until saturation (V), the quantity of nickel retained (Q), the specific (per gram of adsorbent) quantity of nickel retained (Qe), the ratio between the moles of Ni^{2+} adsorbed and the total fed (mmol Ni t/sat), and the removal percentage.

From the data in Table 6, it can be deduced that the SS+D system can treat 447 cm3 of a 30 mg L-1 solution of Ni2+ before reaching total saturation, thereby achieving the highest value for this criterion, surpassing the MM+D system by approximately 60% and the D system by almost 300%. Regarding the amount of sorbate, the SS+D system again retained the largest amount, as in the previous result, followed by the MM+D system, which retained 0.030 mmol Ni2+, and finally, the D system retained 0.0094 mmol. So, the supported system exceeds the MM+D system by more than 2 times and the D system by almost 9 times. In all tests, the SS+D system showed the best adsorbent performance.

Table 6. Test results according to the volume of solution fed until saturation of each filling

System	*V* [mL]	Q [mmol]	Q_e [mmol g^{-1}]	mmol Ni t/sat	Removal [%]
D	114	$9.4 \cdot 10^{-3}$	$6.84 \cdot 10^{-4}$	0.0555	16.9
MM+D	273	$3.0 \cdot 10^{-2}$	$2.20 \cdot 10^{-3}$	0.1330	22.8
SS+D	447	$8.1 \cdot 10^{-2}$	$5.87 \cdot 10^{-3}$	0.2046	39.4

Regarding filler analysis, iron concentration was not detectable for fractions 2, 3 and 4, and total iron was present at 99.9% in fraction 1. According to this result, we infer that there was no migration of the nanoparticles throughout the reactor. Iron from nanoparticles in SS was retained in the initial fraction, thereby addressing the problem of their retention in continuous bed reactors.

The analysis indicated that fraction 1 removed 77.8% of the total Ni2+ adsorbed by the system and yielded q = 0.0088 mmol g-1, the largest value in the reactor, approximately 50% larger than the system's mean. The remaining fractions gave similar values across all the analysed aspects. This result is extremely important because the main problem with the use of

nanoparticles in continuous systems is their retention, which can lead to environmental damage. These results show that the SS material obtained is not only efficient for nickel removal but is also environmentally safe. These are the main advantages of the proposed material, combined with its magnetic separation characteristics. On the other hand, recovering the removed nickel could be costly, so studies on the most environmentally friendly recovery method are needed.

CONCLUSION

The synthesis of nanoparticles on dolomite was achieved in a simple, low-cost manner. It allows a more even distribution of nanoparticles by adding the adsorptive capacity of both materials. This supported system yielded an efficient, environmentally safe material for removing Ni2+, making it a promising material for the development of large-scale treatment reactors, bypassing the obstacle of retaining nanoparticles. In this way, this material can serve as a trigger for the synthesis of other materials of the same type and can also be used to remove other toxic cations.

ACKNOWLEDGMENT

To the University of Buenos Aires for the financing UBACyT N° 20020220300235BA and 20020190100323BA.

REFERENCES

1. R. T. Di Giulio and M. C. Newman, Ecotoxicology, *Casarett and Doull's. Toxicology. The basic science of poisons*, 7th ed., C. D. Klaasen, Ed. New York, USA: McGraw-Hill, 2008.
2. J. Liu, R. A. Goyer, and M. P. Waalkes, Toxic effects of metals., *Casarett and Doull's.Toxicology. The Basic Science of Poisons.*, 7th ed., C. D. Klaasen, Ed. New York, USA: McGraw-Hill, 2008.
3. IARC (International Agency for Research on Cancer), A review of human carcinogens., *Monographs on the evaluation of the carcinogenic risk of chemicals in humans.*, vol. 100C. Lyon, France, 2012, https://publications.iarc.who.int/Book-And-Report-Series/Iarc-Monographs-On-The-Identification-Of-Carcinogenic-Hazards-To-Humans/Review-Of-Human-Carcinogens-Package-Of-6-Volumes-A-B-C-D-E-F--2012, [Accessed: Mar. 18, 2026].
4. C. T. Horngren, S. M. Datar, and M. V Rajan, *Cost accounting: A managerial approach (in Spanish).*, 14th ed. Mexico: Ed. Pearson, 2012.
5. A. Dąbrowski, Z. Hubicki, P. Podkościelny, and E. Robens, Selective removal of the heavy metal ions from waters and industrial wastewaters by ion-exchange method, *Chemosphere*, Vol. 56, No. 2, pp 91–106, 2004, https://doi.org/10.1016/j.chemosphere.2004.03.006.
6. S. Shin and J. Jang, Thiol containing polymer encapsulated magnetic nanoparticles as reusable and efficiently separable adsorbent for heavy metal ions, *Chemical Communications*, No. 41, pp 4230–4232, 2007, https://doi.org/10.1039/B707706H.
7. A. B. Fossati, M. M. Alho, and S. E. Jacobo, Covalent functionalized magnetic nanoparticles for crude oil recovery, *Mater. Chem. Phys.*, Vol. 238, p 121910, 2019, https://doi.org/10.1016/j.matchemphys.2019.121910.
8. A. Bhatnagar, M. Sillanpää, and A. Witek-Krowiak, Agricultural waste peels as versatile biomass for water purification – A review, *Chemical Engineering Journal*, Vol. 270, pp 244–271, 2015, https://doi.org/10.1016/j.cej.2015.01.135.
9. M. Maletin, J. Nikić, V. Gvoić, J. Pešić, Ž. Cvejić, A. Tubić, and J. Agbaba, Optimization and Efficiency of Novel Magnetic-Resin-Based Approaches for Enhanced Nickel Removal from Water, *Processes*, Vol. 12, p 2287, 2024, https://doi.org/10.3390/pr12102287.

10. X. Chen, J. Li, and Z. Yan, Efficient heavy metal removal from aluminum alloy anodizing wastewater using a novel magnetic nanocomposite adsorbent, *J. Mol. Struct.*, Vol. 1351, p 144282, 2026, https://doi.org/10.1016/j.molstruc.2025.144282.
11. A. Hernández-Palomares, F. Mares-Briones, Y. Medrano, F. Espejel-Ayala, F. J. Bacame-Valenzuela, H. N. Böhnel, and R. Esparza, Synthesis of magnetic zeolite from volcanic rock 'Red Tezontle' for removal of Nickel(II) and Copper(II) ions from aqueous solution, *Inorg. Chem. Commun.*, Vol. 186, p 116160, 2026, https://doi.org/10.1016/j.inoche.2026.116160.
12. T. Ngulube, J. R. Gumbo, V. Masindi, and A. Maity, An update on synthetic dyes adsorption onto clay based minerals: A state-of-art review, *Journal of Environmental Management*, Vol. 191. Academic Press, pp 35–57, 2017, https://doi.org/10.1016/j.jenvman.2016.12.031.
13. M. A. Ajala, A. S. Abdulkareem, J. O. Tijani, and A. S. Kovo, Adsorptive behaviour of rutile phased titania nanoparticles supported on acid-modified kaolinite clay for the removal of selected heavy metal ions from mining wastewater, *Appl. Water Sci.*, Vol. 12, No. 2, 2022, https://doi.org/10.1007/s13201-021-01561-8.
14. B. Liu, L. Zhang, K. Ning, and W. Yang, Biochar with nanoparticle incorporation and pore engineering enables enhanced heavy metals removal, *J. Environ. Chem. Eng.*, Vol. 11, No. 5, p 111056, 2023, https://doi.org/10.1016/j.jece.2023.111056.
15. S. Feng, X. Cao, W. Zheng, X. Yue, X. Li, S. Li, X. Wang, and S. Feng, In-situ formed Prussian blue nanoparticles supported by porous biochar as highly efficient removal of cesium ions, *J. Environ. Chem. Eng.*, Vol. 10, No. 3, p 107972, 2022, https://doi.org/10.1016/j.jece.2022.107972.
16. B. Li, M. Li, P. Zhang, Y. Pan, Z. Huang, and H. Xiao, Remediation of Cd (II) ions in aqueous and soil phases using novel porous cellulose/chitosan composite spheres loaded with zero-valent iron nanoparticles, *React. Funct. Polym.*, Vol. 173, p 105210, 2022, https://doi.org/10.1016/j.reactfunctpolym.2022.105210.
17. Y. Zhu, W. Shi, H. Gao, C. Li, W. Liang, Y. Nie, C. Shen, and S. Ai, A novel aminated lignin/geopolymer supported with Fe nanoparticles for removing Cr(VI) and naphthalene: Intermediates promoting the reduction of Cr(VI), *Science of The Total Environment*, Vol. 866, No. 10, p 161379, 2023, https://doi.org/10.1016/j.scitotenv.2022.161379.
18. D. T. Nayak, V. K. Raja, G. Arthanareeswaran, T. D. Khoa, and W. Taweepreda, A high-performance nanofiltration membrane synthesized by embedding amino acids and ionic liquids in cellulose acetate for heavy metal separation, *RSC Sustainability*, Vol. 3, No. 4, pp 1966–1981, Feb. 2025, https://doi.org/10.1039/d4su00688g.
19. R. Hou, P. Wang, C. Cheng, J. Dai, W. Yan, Y. Zhou, and C. Gao, Construction of a gradient cross-linked nanofiltration membrane with quaternized surface for efficient heavy metal removal, *Desalination*, Vol. 614, p 119169, 2025, https://doi.org/10.1016/j.desal.2025.119169.
20. S. H. Huang and D. H. Chen, Rapid removal of heavy metal cations and anions from aqueous solutions by an amino-functionalized magnetic nano-adsorbent, *J. Hazard. Mater.*, Vol. 163, No. 1, pp 174–179, 2009, https://doi.org/10.1016/j.jhazmat.2008.06.075.
21. S. S. Banerjee and D.-H. Chen, Fast removal of copper ions by gum arabic modified magnetic nano-adsorbent, *J. Hazard. Mater.*, Vol. 147, No. 3, pp 792–799, 2007, https://doi.org/10.1016/j.jhazmat.2007.01.079.
22. A. El Mouden, N. El Messaoudi, A. El Guerraf, A. Bouich, V. Mehmeti, A. Lacherai, A. Jada, and J. H. Pinê Américo-Pinheiro, Removal of cadmium and lead ions from aqueous solutions by novel dolomite-quartz@Fe3O4 nanocomposite fabricated as nanoadsorbent, *Environ. Res.*, Vol. 225, p 115606, 2023, https://doi.org/10.1016/j.envres.2023.115606.

23. M. N. Piol, A. Acuña Alfonso, A. Saralegui, and C. Vazquez, Adsorption competition study between chromate and phosphate from their solutions by total reflection Xray fluorescence spectrometry, *Xray Spectrom.*, Vol. 50, No. 1, pp 21–27, 2021, https://doi.org/10.1002/xrs.3186.
24. M. N. Piol, C. Dickerman, M. P. Ardanza, A. Saralegui, and S. P. Boeykens, Simultaneous removal of chromate and phosphate using different operational combinations for their adsorption on dolomite and banana peel, *J. Environ. Manage.*, Vol. 288, p. 112463, 2021, https://doi.org/10.1016/j.jenvman.2021.112463.
25. S. P. Boeykens, M. N. Piol, L. Samudio Legal, A. B. Saralegui, and C. Vázquez, Eutrophication decrease: Phosphate adsorption processes in presence of nitrates, *J. Environ. Manage.*, Vol. 203, pp 888–895, 2017, https://doi.org/10.1016/j.jenvman.2017.05.026.
26. S. Boeykens, A. Saralegui, N. Caracciolo, and M. N. Piol, Agroindustrial Waste for Lead and Chromium Biosorption, *Journal of Sustainable Development of Energy, Water and Environment Systems*, Vol. 6, No. 2, pp 341–350, 2018, https://doi.org/10.13044/j.sdewes.d5.0184.
27. H. P. Boehm, Chemical Identification of Surface Groups, in *Advances in Catalysis*, Vol. 16, D. D. Eley, H. Pines, and P. B. Weisz, Eds. Academic Press, 1966, pp 179–274.
28. J. Vallini, V. Willson, L. Fernández Luco, A. B. Saralegui, S. P. Boeykens, and M. N. Piol, Demolition waste for adsorption of metals: A step towards the circular economy, *J. Environ. Manage.*, Vol. 342, p. 118200, 2023, https://doi.org/10.1016/j.jenvman.2023.118200.
29. APHA, AWWA, and WEF and R. Baird Eaton A. Rice E.W., *Standard Methods for the Examination of Waters and Wastewaters*, 23rd ed. Washington: American Public Health Association; American Water Works Association; Water Environment Federation, 2017.
30. I. Langmuir, The adsorption of gases on plane surfaces of glass, mica and platinum, *Journal of the American Chemical Society*, Vol. 40, No. 9, pp 1361–1403, 1918, https://doi.org/10.1021/ja02242a004.
31. H. M. F. Freundlich, Over the Adsorption in Solution, *J. Phys. Chem.*, Vol. 57, pp 385–471, 1906, https://doi.org/10.1515/zpch-1907-5723.
32. S. Lagergren, About the theory of so-called adsorption of soluble substances (in German: Zur theorie der sogenannten adsorption gelosterstoffe), *Supplement of the Royal Swedish Science Academiens Documents (in Swedish: BihangTill Konglinga Svenska Vetenskaps Academiens Handlingar)*, Vol. 24, No. 2, pp 1–39, 1898, https://doi.org/10.1007/BF01501332.
33. Y. S. Ho and G. McKay, Pseudo-second order model for sorption processes, *Process Biochemistry*, Vol. 34, pp 451–465, 1999, https://doi.org/10.1016/S0032-9592(98)00112-5.
34. A. Saralegui, M. N. Piol, V. Willson, N. Caracciolo, and S. Boeykens, Lignocellulosic Waste as Adsorbent for Water Pollutants. A Step towards Sustainability and Circular Economy, Chapter 3. pp 168-184.In: *Bioremediation of Toxic Metal(loid)s*, 1st ed., Malik A., Kidwai M.K., and Garg V.K., Eds. CRC Press, 2022.
35. T. Lopez, Iron nanoparticles supported on a low-cost material: synthesis and application as a metal adsorbent (in Spanish). *Chemical Engineering Graduate thesis*, Facultad de Ingeniería, Universidad de Buenos Aires, Argentina, 2024, https://campusgrado.fi.uba.ar/course/view.php?id=485&section=40#tabs-tree-start, [Accessed: Mar. 18, 2026].
36. O. Levenspiel, *Chemical reaction engineering*. Chapter 13, pp 293-320. Wiley, 1999.
37. H. C. Thomas, Heterogeneous Ion Exchange in a Flowing System, *J. Am. Chem. Soc.*, Vol. 66, No. 10, pp 1664–1666, 1944, https://doi.org/10.1021/ja01238a017.

38. G. S. Bohart and E. Q. Adams, Some aspects of the behavior of charcoal with respect to chlorine, *J. Am. Chem. Soc.*, Vol. 42, No. 3, pp 523–544, 1920, https://doi.org/10.1021/ja01448a018.
39. Y. H. Yoon and J. H. Nelson, Application of Gas Adsorption Kinetics I. A Theoretical Model for Respirator Cartridge Service Life, *Am. Ind. Hyg. Assoc. J.*, Vol. 45, No. 8, pp 509–516, 1984, https://doi.org/10.1080/15298668491400197.
40. A. B. Fossati, M. M. Alho, and S. E. Jacobo, Polymer-functionalized nanoparticles for improving oil displacement, *Advances in Natural Sciences: Nanoscience and Nanotechnology*, Vol. 9, No. 1, p. 15007, 2018, https://doi.org/10.1088/2043-6254/aaa6e8.
41. O. Sivrikaya, A study on the physicochemical and thermal characterisation of dolomite and limestone samples for use in ironmaking and steelmaking, *Ironmaking & Steelmaking*, Vol. 45, No. 8, pp 764–772, 2018, https://doi.org/10.1080/03019233.2017.1337264.
42. R. Janani, B. Gurunathan, K. Sivakumar, and P. Senthilkumar, Strychnos potatorum seeds derived magnetic graphene oxide nanocomposite for removal of nickel from wastewater: Adsorption performance, isotherm, kinetic and desorption behavior, *Desalination Water Treat.*, Vol. 319, p. 100463, 2024, https://doi.org/10.1016/j.dwt.2024.100463.
43. C. D. Bahl, M. C. Gely, and A. Pagano, Flow Patterns in Chemical Reactors: Development of Mathematical and Numerical Models Based on CFD (in Spanish), *Mecánica Computacional*, Vol. XXI, No. 2, pp 49–68, 2012, https://www.amcaonline.org.ar/ojs, [Accessed: Mar. 18, 2026].

Paper submitted: 11.12.2025
Paper revised: 20.03.2026
Paper accepted: 24.03.2026